Higher neuronal discharge rate in the motor area of the subthalamic nucleus of Parkinsonian patients

Marc Deffains, Peter Holland, Shay Moshel, Fernando Ramirez de Noriega, Hagai Bergman, Zvi Israel

Higher neuronal discharge rate in the motor area of the subthalamic nucleus of Parkinsonian patients

Marc Deffains [1,2,*], Peter Holland [3,*], Shay Moshel [1,2,4], Fernando Ramirez de Noriega [5], Hagai Bergman [1,2] & Zvi Israel [5]

1 Department of Medical Neurobiology, The Hebrew University-Hadassah Medical School, Jerusalem, 91120, Israel

2 The Edmond and Lily Safra Center for Brain Sciences, The Hebrew University, Jerusalem, 91904, Israel

3 Alpha Omega Engineering Ltd, Nazareth, 1612102, Israel

4 The Research Laboratory of Brain Imaging and Stimulation, The Jerusalem Mental Health Center, Kfar-Shaul Etanim, The Hebrew University-Hadassah Medical School, Jerusalem, 91060, Israel

5 Center for Functional and Restorative Neurosurgery, Department of Neurosurgery, Hadassah University Hospital, Jerusalem, 91120, Israel

* *Equal contribution*

Corresponding author : Marc Deffains

Department of Medical Neurobiology (physiology), The Hebrew University-Hadassah Medical School, POB 12272, Jerusalem, 91120, Israel. Email: marcd@ekmd.huji.ac.il

Abbreviated title : Abnormal subthalamic discharge rate

Abstract

In Parkinson's disease, pathological synchronous oscillations divide the subthalamic nucleus (STN) of patients into a dorsolateral oscillatory region and ventromedial non-oscillatory region. This bipartite division reflects the motor vs. the non-motor (associative/limbic) subthalamic areas, respectively. However, significant topographic differences in the neuronal discharge rate between these two STN sub-regions in Parkinsonian patients is still controversial.

In this study, 119 STN microelectrode trajectories (STN length > 2mm, mean = 5.32mm) with discernible oscillatory and non-oscillatory regions were carried on 60 patients undergoing deep brain stimulation surgery for Parkinson's disease. 2137 and 2152 multi-unit stable signals were recorded (recording duration > 10s, mean = 21.25s) within the oscillatory and non-oscillatory STN regions, respectively. Spike detection and sorting was applied offline on every multi-unit stable signal using an automatic method with systematic quantification of the isolation quality (range = 0 to 1) of the identified units. In all, 3094 and 3130 units were identified in the oscillatory and non-oscillatory regions, respectively.

On average, the discharge rate of better-isolated neurons (isolation score > 0.70) was higher in the oscillatory region than the non-oscillatory region (44.55 ± 0.87 versus 39.97 ± 0.77 spikes/s, N = 665 and 761, respectively). The discharge rate of the STN neurons was positively correlated to the strength of their own and their surrounding 13-30Hz beta oscillatory activity.

Therefore, in the Parkinsonian STN, beta oscillations and higher neuronal discharge rate are correlated and coexist in the motor area of the STN compared to its associative/limbic area.

Keywords: subthalamic nucleus; Parkinson's disease; deep brain stimulation; microelectrode recording; neuronal discharge

Introduction

In Parkinson's disease (PD), dysregulation of the activity within the subthalamic nucleus (STN) may consist of changes in discharge rate, pattern and synchronization of activity (Brown 2003; Moshel et al. 2013). Electrophysiological recordings in monkeys (Bergman et al. 1994; Wichmann et al. 1994; Wichmann and Saores 2006) have shown a modest increase in the neuronal discharge rate in the STN after 1-methyl-4-phenyl-1,2,3,6-tetrahydropyridine (MPTP) intoxication. In Parkinsonian patients undergoing deep brain stimulation (DBS), the discharge rate of STN neurons is similar to that described in MPTP-treated monkeys (Magarinos-Ascone et al. 2000; Rodriguez-Oroz et al. 2001; Steigerwald et al. 2008; Remple et al. 2011). In addition, the STN neuronal discharge rate in Parkinsonian patients is higher than in patients suffering from essential tremor without Parkinsonian symptoms (Steigerwald et al. 2008).

Many electrophysiological studies in both MPTP-treated monkeys (Bergman et al. 1994; Raz et al. 2000; Stein and Bar-Gad 2013) and Parkinsonian patients (Hutchison et al. 1997; Levy et al. 2000, 2001, 2002) have also reported abnormal synchronized oscillatory activity of STN neurons at different frequencies ranging from 3 to 30Hz. Besides, such neuronal oscillations have been observed in local field potentials (LFPs) recorded within the STN of the 6-hydroxydopamine-lesioned rodent model of PD (Sharrot et al. 2005; Mallet et al. 2008) and Parkinsonian patients (Brown 2003).

Remarkably, earlier studies have shown that abnormal oscillations within the STN of Parkinsonian patients are limited to its dorsolateral region, thus dividing the STN into a dorsolateral oscillatory region (DLOR) and ventromedial non-oscillatory region (VMNR) (Kuhn et al. 2005; Moran et al. 2008; Zaidel et al. 2009, 2010; Seifreid et al. 2012;

Lourens et al. 2013). Such an electrophysiological division overlaps with the functional motor and associative/limbic areas of the STN, respectively (Haber et al. 1993; Karachi et al. 2005; Benarroch 2008; Mathai and Smith 2011; Haynes and Haber 2013).

However, comparison of the neuronal discharge rate between the dorsolateral part and the ventromedial part of the STN of Parkinsonian patients provides inconsistent results (Seifreid et al. 2012; Lourens et al. 2013). Additionally, the precise relationship between the neuronal discharge rate and the neuronal oscillations in the STN of Parkinsonian patients is still elusive. To address these issues, we identified single-unit activity from the multi-unit signals recorded within the STN of Parkinsonian patients undergoing STN-DBS surgery. Spike detection and sorting was performed offline using a fully automatic method with systematic quantification of the isolation quality of the identified units (Joshua et al. 2007). Then, we compared the mean neuronal discharge rate between the DLOR and VMNR, as a function of the isolation quality of the units. Finally, we examined how the discharge rate of the STN neurons recorded in both STN sub-regions varied depending on the strength of their own oscillatory activity as well as the strength of their surrounding oscillatory activity (i.e. multi-unit oscillatory activity recorded in the vicinity of the microelectrode) at different frequencies.

Materials and Methods

Patients and surgery

Data were collected from 60 Parkinsonian patients undergoing STN-DBS surgery (48 bilateral and 12 unilateral) at the Hadassah medical center, Jerusalem, Israel, between January 2009 and March 2012. Patients (44 males and 16 females) were 61.2 ± 7.2 years

old and with disease duration of 10.1 ± 4.9 years (mean ± standard deviation, SD). Individual information regarding the patients is given in table 1. All patients accepted criteria for STN-DBS and signed a written informed consent for surgery that involved microelectrode recording. This study was authorized and approved by the Institutional Review Board of Hadassah Hospital in accordance with the Helsinki Declaration (reference codes: 0545-08-HMO and HMO: 10-18.01.08).

Surgery was performed using a CRW stereotactic frame (Radionics, Burlington, MA, USA). STN target coordinates were chosen as a composite of indirect anterior commissure-posterior commissure (AC-PC) atlas-based location and direct (1.5 or 3Tesla) T2 magnetic resonance imaging, using Framelink 4 or 5 software (Medtronic, Minneapolis, USA). All recordings used in this study were made while the patients were fully awake (not sedated). The patient's level of awareness was continuously assessed clinically, and if drowsy, the patient was stimulated and awoken through conversation by a member of the clinical team. Data were collected while the patients were off dopaminergic medication (overnight washout > 12 hours).

Microelectrode recordings and recording stability inclusion criteria

Microelectrode recordings were carried out to optimize the placement of the DBS contacts in the STN. Data were acquired with the MicroGuide system (AlphaOmega Engineering, Nazareth, Israel). Neurophysiological activity was recorded via polyamide coated tungsten microelectrodes with an impedance of 0.57 ± 0.12MΩ at 1kHz (AlphaOmega Engineering, Nazareth, Israel). The signal was amplified by 10000, band-passed filtered from 250 to 6000Hz, using a hardware four-pole Butterworth filter and

sampled at 48kHz by a 12-bit A/D converter (using ± 5V input range). For every recording session, a microelectrode recording exploration using two microelectrodes was made starting 10mm above the estimated center of the STN target, based on the pre-operative T2 MRI image. Every microelectrode trajectory followed a double-oblique approach (~ 60º from the axial AC-PC plane and 15º from the mid-sagittal plane) towards the dorsolateral STN target. The final trajectory was slightly modified, based on the pre-operative T1 MRI image, to avoid the cortical sulci, the ventricles and major blood vessels (Machado et al. 2006). The "central" electrode was directed at the center of the STN target and the "anterior" electrode was located 2mm anterior/ventral to the central electrode in the parasagittal plane. The microelectrodes were simultaneously advanced in small discrete steps (step size ranged from 400 to 50μm) toward and through the STN to identify the upper and lower borders of the STN and multi-unit signals were recorded between each step (recording started 2s after the end of the movement). Typically, shorter steps (~100μm) were used as the electrode was advanced closer to the presumed location of the STN. In this study, STN borders and its sub-regions (DLOR and VMNR) were automatically detected, ex post facto, using the Hidden Markov Model method (Zaidel et al. 2009).

A total of 108 microelectrode electrophysiological explorations (from 48 bilaterally and 12 unilaterally implanted Parkinsonian patients with two microelectrodes per exploration) were analyzed. Some of the electrophysiological explorations were made by a single microelectrode (N = 7) to accommodate for cortical anatomy under the burr hole, yielding a total of 209 microelectrodes trajectories aiming at the STN. Out of the 209 microelectrode trajectories, all 119 microelectrode trajectories that passed the inclusion

criteria of the study, namely a clearly defined STN entry and exit and discernible DLOR and VMNR, were included in the analysis database. These 119 microelectrode trajectories traversed > 2mm of STN (94% traversed > 3mm of STN), with a mean STN length of 5.32 ± 1.19mm and a mean percentage of STN-DLOR of 48.20 ± 22.21% (mean ± SD). The microelectrode trajectory characteristics are given in table 2. All the multi-unit signals recorded within the STN while the patient underwent voluntary and passive joint movements were excluded so as not to distort the STN spontaneous neuronal activity by the STN neuronal responses to those passive joint movements.

Every STN multi-unit signal was subjected to stability inspection using custom-made software (Zaidel et al. 2010). To do so, each multi-unit trace was divided into consecutive segments of 25ms using a sliding window (step size = 5ms) and the root mean square (RMS) of the multi-unit trace was computed for each windowed segment. A section of the trace was considered unstable when at least 5 consecutive segments had RMS values that exceeded 3-fold the SD of the median RMS. The longest stable section of the trace was selected for further analysis while the rest of the trace was discarded. The selection parameters (window size, number and amplitude of deviation) were chosen following visual inspection of the data. Only stable sections longer than 10s were automatically selected for further analysis. A total of 4289 stable STN multi-unit signals were studied (mean ± SD recording span = 21.25 ± 19.17s).

Automatic offline spike sorting and quantification of isolation quality of identified units

Single-unit STN activity was assessed by sorting spike trains from every stable multi-unit signal (with a duration longer than 10s) via an automatic offline spike detection and

sorting method (see review by Lewicki 1998) developed in collaboration with AlphaOmega Inc (AlphaOmega Engineering, Nazareth, Israel). Spikes were detected using a positive and negative voltage bandwidth threshold trigger. The lower and upper thresholds of the bandwidth threshold trigger were automatically set as 3.3 and 15 SDs of the stable multi-unit signal (namely only signals with amplitudes larger than 3.3 SDs but lower than 15 SDs, for artifact rejection, were included). All the detected spikes (duration of a detected spike segment = 2ms, 96 sampling points) were aligned to their minimum point in order to prevent double detection of spikes by both the positive and negative voltage thresholds and to aid in feature extraction and clustering. Salient features of the detected spikes were extracted with principal component analysis, using the scores of the first three principal components as features for clustering. Identification of different spike clusters reflecting the activity of different units was accomplished via the k-means clustering method, using the silhouette method and the Dunn Index (Dunn 1973; Rousseeuw 1987) to determine the optimal number of clusters between the limits of 1 and 5. Clusters representing less than 10% of the total spike count or comprised of fewer than 100 spikes were removed from further analysis. In order to avoid the inclusion of two or more separate clusters which in fact represented a single unit, a template matching approach was used based on the mean spike template extracted from each cluster. The time points of template matches from each potential unit were calculated and if any unit shared more than 15% of matches with any other potential unit these clusters were merged into a single unit.

The isolation quality of the units identified by the spike sorter software was systematically graded by measuring their isolation scores (Joshua et al. 2007). The

isolation score ranges from 1 (i.e. perfect isolation) to 0 (i.e. highly noisy multi-unit activity). Figure 1.A shows examples of STN multi-unit activities (left and middle). The right plots show the superimposed waveforms of 100 randomly selected waveforms of the extracellular action potentials of an identified unit sorted from its multi-unit activity. The units in figure 1.A are ordered as a function of the isolation score of the unit.

Power spectral density analysis and oscillation strength measurement (Oscil.Score)

The Z-score normalization process was applied to the raw analog signal (selected stable section) to obtain an unbiased estimate (by the amplitude of the recorded neuronal activity) of the oscillatory activity (Zaidel et al. 2010). The Z-normalized signal was rectified by the "absolute" operator (Moran et al. 2008; Moran and Bar-Gad 2010; Zaidel et al. 2010). The rectified signal follows the envelope of the multi-unit activity and therefore allows the detection of burst frequencies below the range of the operating room band-pass filter (250-6000Hz). Since the LFP frequency domain was filtered out by the recording apparatus, the resulting power spectrum density (PSD) only represented spiking activity. The PSD of each signal was calculated using Welch's method with a 1.5s hamming window (50% overlap) and a spectral resolution of 1/3Hz (nfft = 144231, sampling frequency = 48000Hz). Any DC component generated by the "absolute" operator was removed by subtracting the mean of every windowed segment of the rectified signal. Similarly, we also calculated the PSD of the single STN units identified by the spike sorter software. To do so, for each identified unit, the spike train (i.e. time epochs of the detected spikes) was low-passed filtered (cutoff frequency = 100Hz) and the PSD of every Z-normalized spiking activity was calculated using Welch's method

(see above for the parameters), without prior rectification by the absolute operator. The mean PSD of the STN populations was defined as the average of the PSD of all units/signals calculated over the 3-75Hz range.

Measurement of the strength of the oscillatory activity for every unit and multi-unit signal was carried out by computing the *Oscil.Score* (Moshel et al. 2013). Briefly, all calculations were performed in the frequency range of 3 to 75Hz. For every PSD, the peak value of the PSD was calculated and the *Oscil.Score* was defined as the Z-score amplitude of the PSD peak. The frequency at which the PSD attained its maximal value was defined as f_{peak} (i.e. frequency at which the *Oscil.Score* was calculated).

Software and Statistics

All the data and statistical analyses were done using custom-made MATLAB 7.5 routines (Mathworks, Natick, MA, USA). The neuronal discharge rate between the DLOR and VMNR was compared using a two-sample t-test and if necessary Bonferroni's correction was used to adjust the chosen significance level according to the number of multiple comparisons. Linear (Pearson) and non-linear (Spearman) regression analysis was used to examine the relationship between the discharge rate of the STN units and their isolation score and their multi-unit oscillation strength (*Oscil.Score*). Statistics presented in this report, if not specified, use the mean ± standard error of the mean (SEM) and the criterion for statistical significance was set at $P < 0.05$ for all statistical tests.

Results

Database and spike sorting results

In this study, 119 STN microelectrodes trajectories from 60 Parkinsonian patients were used to yield 4289 multi-unit stable signals that were recorded within the STN. Using the Hidden Markov Model method (Zaidel et al. 2009), out of the 4289 multi-unit signals, 2137 and 2152 were located within the DLOR and VMNR, respectively. A total of 6224 STN units were identified using the spike sorter software on the 4289 multi-unit signals. Out of the 6224 identified STN units, 3094 units were located in the DLOR and 3130 units in the VMNR.

Power spectral density analysis between the DLOR and VMNR

Figure 2.A and 2.B (left) show the mean PSD of STN multi-unit activity of the DLOR and VMNR recordings, respectively. As expected and as previously reported (Kuhn et al. 2005; Moran et al. 2008; Zaidel et al. 2009, 2010; Seifreid et al. 2012), STN sub-regions can be easily differentiated based on neuronal oscillatory activity. The mean PSD of DLOR exhibited 3-7Hz theta, 8-12Hz alpha and 13-30Hz beta oscillatory activity with peaks at 4.67, 11.33 and 23.33Hz, respectively and no obvious >30Hz gamma activity. In contrast, the mean PSD of VMNR presented reduced power at the theta, alpha and beta ranges whereas the high-frequency gamma activity seemed to increase compared to DLOR.

Remarkably, the distribution of f_{peak} (i.e. frequency at which the *Oscil.Score* was calculated) in the DLOR and VMNR perfectly fitted with average spectra of the two STN sub-regions. Most of the f_{peak} in the DLOR were distributed within the theta, alpha and

beta frequencies (Fig 2.A, right) whereas in the VMNR, most of the f_{peak} were found in the gamma band (Fig 2.B, right). The median ± median absolute deviation (MAD) of f_{peak} distribution equaled 18.33 ± 11.83Hz and 41 ± 19.76Hz, in the DLOR and VMNR, respectively.

Neuronal discharge rate between the DLOR and VMNR as a function of the isolation quality of the sorted units

For every STN unit, the neuronal discharge rate and isolation score were calculated. Figure 1.B gives the distribution of the isolation score of all the identified units. Scatter plots of the neuronal discharge rate and isolation score of all the units located in the DLOR (Fig. 3.A) and VMNR (Fig. 3.B) were built. The mean isolation score was 0.35 ± 0.33 and 0.39 ± 0.33 (mean ± SD) in the DLOR and VMNR, respectively. Remarkably, a significant positive correlation between neuronal discharge rate and isolation score was found in both the DLOR (Pearson's $r = 0.42$, Spearman's $r = 0.50$, $P < 0.001$) and the VMNR (Pearson's $r = 0.37$, Spearman's $r = 0.44$, $P < 0.001$), indicating that units with the lowest isolation scores had the lowest discharge rates, regardless of STN sub-regions.

Spike detection and sorting process can be affected by two types of error that differentially affect the calculated discharge rate. False negative errors, namely misses of real spikes, decrease the calculated discharge rate. On the other hand, false positive errors, namely erroneously classifying noise events as spikes, lead to an artificial increase in the discharge rate of the detected units. The positive correlation between the discharge rate of the detected units and their isolation quality indicates that the spike detection and

sorting algorithm used in this study tended to miss spikes (false negatives) rather than erroneously classify noise events as spikes (false positives).

Inspection of the scatter plots of the discharge rate and isolation score of the STN detected units (Fig.3.A and 3.B) revealed a stabilization of the correlation between the discharge rate and isolation scores around isolation score of 0.40. Therefore, we binned all the units with an isolation score above 0.40 as a function of their isolation score range. The mean discharge rate of the STN neurons for the different isolation score bins in the DLOR and VMNR is shown Figure 3.C. In both STN sub-regions, the mean neuronal discharge rate decreased while the isolation score increased when isolation score ranged between 0.71 and 1.0 (namely for the better-isolated units). Moreover, for isolation scores above 0.70, the mean neuronal discharge rate in the DLOR was systematically significantly higher (two-sample t-test, $P < 0.05$) than in the VMNR (Fig.3.C).

Neuronal discharge rate between the DLOR and VMNR as a function of neuronal oscillatory activity

The impact of neuronal oscillatory activity on the neuronal discharge rate in both the DLOR and VMNR was assessed only for the better-isolated units (i.e. isolation score > 0.70). These STN units (665 and 761 in DLOR and VMNR, respectively) fired on average at a higher rate in the DLOR than in the VMNR (Fig.3.C). To ensure that oscillatory features of the surrounding multi-unit activity reflected those of the single-unit activity in both STN sub-regions, we calculated the mean PSD of STN single-unit activity for the better-isolated units recorded in the DLOR and VMNR. For both STN

sub-regions, the mean PSD of STN single-unit activity exhibited the same oscillatory features as those of the mean PSD of STN multi-unit activity (data not shown).

Figure 4 depicts the mean neuronal discharge rate of the better-isolated units according to the f_{peak} range of their surrounding multi-unit oscillatory activity (3-7Hz theta range, 8-12Hz alpha range, 13-30Hz beta range and 30-75Hz gamma band). Pairwise comparisons between the DLOR and VMNR mean discharge rates as a function of the f_{peak} range only revealed a significantly higher neuronal discharge rate for the units in the DLOR compared to the VMNR, for f_{peak} in the 13-30Hz beta range (two-sample t-test with Bonferroni's correction for multiple comparisons, $P < 0.001$, 44.25 ± 1.35 and 34.27 ± 2.12 spikes/s, respectively). Therefore, the higher neuronal discharge rate in the DLOR compared to the VMNR appears to be surrounding 13-30Hz beta oscillatory activity-specific. Keeping with this view, we found that the mean neuronal discharge rate in the DLOR was only higher than in the VMNR when the f_{peak} of the single-unit oscillatory activity ranged in the 13-30Hz beta frequencies (two-sample t-test with Bonferroni's correction for multiple comparisons, $P < 0.001$, 48.18 ± 1.84 and 33.89 ± 3.15 spikes/s, respectively).

Remarkably, the linear regression analysis between the discharge rate of the units and the *Oscil.Score* of their surrounding oscillatory activity only showed a significant positive correlation between these two variables for f_{peak} in the 3-7Hz theta range (Pearson's $r = 0.16$, Spearman's $r = 0.14$, $P < 0.01$, Fig.5.A) and in the 13-30Hz beta range (Pearson's $r = 0.20$, Spearman's $r = 0.22$, $P < 0.001$, Fig.5.C). In addition, for f_{peak} in 13-30Hz beta range the mean *Oscil.Score* was significantly higher in the DLOR than in the VMNR (two-sample t-test, $P < 0.001$, 4.22 ± 0.07 and 3.37 ± 0.09, respectively, Fig.5.C,

inset). Therefore, this linear regression analysis provides support for the finding of a higher neuronal discharge rate in the DLOR than in the VMNR for surrounding oscillatory activity at the 13-30Hz beta frequency. The analysis conducted on the single-unit oscillatory activity rather than on the multi-unit oscillatory activity yielded the same qualitative results. Indeed, we found that the discharge rate of the neurons was only positively correlated to the *Oscil.Score* of their single-unit oscillatory activity for f_{peak} in the 3-7Hz theta range (Pearson's r = 0.25, Spearman's r = 0.23, P < 0.001) and in the 13-30Hz beta range (Pearson's r = 0.25, Spearman's r = 0.26, P < 0.001). In addition, the mean *Oscil.Score* of single-unit beta oscillatory activity was also significantly higher in the DLOR than in the VMNR (two-sample t-test, P < 0.001, 3.95 ± 0.08 and 3.33 ± 0.11, respectively).

Discussion

In this report, we used the oscillatory properties of STN neurons of each patient to divide the STN into two electrophysiological sub-regions. We demonstrated that neurons fired at a higher rate in the DLOR of the Parkinsonian STN compared to the VMNR and stressed the necessary of objective and graded quantification of the isolation quality of the units in studies using extracellular recordings and spike detection and sorting protocols. We found that the higher neuronal discharge rate in the DLOR compared to the VMNR could be detected for the better-isolated units (i.e. isolation score > 0.70). Moreover, we showed that this STN region-specific higher neuronal discharge rate was correlated to the beta oscillatory activity of the units and the multi-unit signals recorded in the area surrounding the neurons.

A higher neuronal discharge rate in the DLOR than in the VMNR of the Parkinsonian STN - Implications for the pathophysiology of Parkinsonian motor symptoms

Taking into account only the better-isolated units (i.e. isolation score > 0.70), the mean neuronal discharge rate in the STN (1426 STN units, DLOR and VMNR included) of our Parkinsonian patients was 42.11 ± 0.58 spikes/s and therefore lies within the range of previous studies in Parkinsonian patients (Hutchison et al. 1998; Magarinos-Ascone et al. 2000; Rodriguez-Oroz et al. 2001; Steigerwald et al. 2008; Remple et al. 2011) and MPTP-treated monkeys (Bergman et al. 1994; Wichmann et al. 1994; Wichmann and Soares 2006). After dividing the STN of Parkinsonian patients into DLOR and VMNR, we found a higher neuronal discharge rate in the DLOR than in the VMNR (44.55 ± 0.87 versus 39.97 ± 0.77 spikes/s, N = 665 and 761, respectively). Seifreid et al. (2012) divided the Parkinsonian STN along the stereotactic z-axis into three parts of equal size, but failed to describe significant topographic differences in the neuronal discharge rate along the dorsoventral plane of the STN. On the contrary, based on the general functional tripartite division of the STN (Haber et al. 1993; Karachi et al. 2005; Benarroch 2008; Mathai and Smith 2011; Haynes and Haber 2013), Lourens et al. (2013) showed that STN neurons of their Parkinsonian patients fire at a higher rate in the suspected dorsal sensorimotor part than in the ventral associative/limbic part. However, they only analyzed 130 STN recording sites from 18 patients and the total number of sorted units was 177 and 71 in the suspected motor and associative/limbic areas, respectively.

In most studies using spike sorting protocols to examine STN single-unit activity (Steigerwald et al. 2008; Remple et al. 2011; Seifreid et al. 2012), the isolation quality of the units is only based on visual inspection and without objective tests (Joshua et al.

2007; Hill et al. 2011). Moreover, the data is divided into well-isolated and multi-unit activity, assuming an unrealistic binary isolation process. Remarkably, Lourens et al. (2013) used advanced methods to quantify the isolation quality of the STN units in an unbiased and standardized manner (only neurons with isolation score > 0.75 were included). In this study, we demonstrated that a higher neuronal discharge rate in the DLOR was only found for the better-isolated neurons (isolation score > 0.70).

Another issue relative to current spike sorting methods of activity recorded by single micro-electrode is the under-estimate of the neuronal discharge rate due to overlapping of the spikes when two neurons fire simultaneously as for instance when the neuronal activity is synchronized (Lewicki et al. 1998). We are fully aware that synchronized activity in the STN is likely to result in an under-estimate of the discharge rate of the STN neurons detected by the spike sorter software. However, recently, Moshel et al. (2013) reported that STN synchronized activity is predominant in the DLOR as compared to the VMNR. Therefore, overlapping spikes would further the null hypothesis of the study, namely no significant difference in the neuronal discharge rate between the two STN sub-regions of PD patients.

Earlier studies have shown that the DLOR overlaps the sensorimotor part of the STN (Rodriguez-Oroz et al. 2001; Zaidel et al. 2010). The VMNR is considered as the associative/limbic part of the STN (Eitan et al. 2013). In PD, midbrain dopaminergic neurons degenerate, leading to a cascade of physiological changes and especially an abnormal increase in STN activity. The STN hyper-activity is postulated to have a pivotal role in the pathophysiology of the motor symptoms in PD (Albin et al. 1989; Bergman et al. 1990; Delong 1990). Histological and human functional imaging studies revealed that

the striatal dopamine depletion is heavier in the posterior putamen than the caudate nucleus and the ventral striatum in PD (Kish et al. 1988; Morrish et al. 1996; Nurmi et al. 2001; Bruck et al. 2006). Anatomically and functionally, the posterior putamen, the caudate nucleus and the ventral striatum correspond to the sensorimotor, associative and limbic parts of the striatum, respectively (Alexander et al. 1986; Parent and Hazrati 1995; Yin and Knowlton 2006). Therefore, the uneven pattern of dopamine loss reported in the striatum of Parkinsonian patients hints that basal ganglia sensorimotor territories such as the motor area of the STN are more strongly impacted than the associative and limbic territories of the basal ganglia in PD. In line with this view, our results based on physiological patient-specific (Zaidel et al. 2010) rather than a general anatomical atlas-based division of STN sub-domains (Lourens et al. 2013) indicate that the neuronal discharge rate is higher in the motor area than in the associative/limbic area of the STN of Parkinsonian patients.

Numerous theoretical and experimental studies have demonstrated that in cortical and other neuronal circuits a balance between excitatory and inhibitory synaptic inputs can emerge (i.e. excitatory and inhibitory synaptic inputs cancel out) and cause the membrane potential to hover near the spike threshold (Shadlen and Newsome 1994; Amit and Brunel 1995; van Vreeswijk and Sompolinsky 1996; Tan et al. 2014). As a result, small fluctuations in the net synaptic input (sum of excitatory and inhibitory inputs) would be sufficient to allow the membrane potential of a neuron to cross the spike threshold and generate spikes. Anatomically, the majority of the afferent synapses to the output structures of the STN (internal and external parts of the globus pallidus and substantia nigra reticulata) are inhibitory GABAergic synapses (Difilgia et al. 1982; Francois et al.

1987; Shink and Smith 1995) and STN is the only excitatory drive of these structures. Therefore, this small but significantly higher neuronal discharge rate in the motor area of the Parkinsonian STN might create a greater imbalance in the net synaptic input (increase of excitatory inputs) of the neurons in the pallidal/nigral motor domain compared to those in the non-motor domain, leading to differential abnormal spiking activity in the functional domains of the output structures of the STN.

Relationship between neuronal discharge rate and neuronal oscillatory activity in the DLOR and VMNR of the Parkinsonian STN

In this study, STN oscillatory activity was investigated from multi-unit activity recorded within the STN of Parkinsonian patients (Moran et al. 2008; Moran and Bar-Gad 2010; Zaidel et al. 2010). Another option was to use the single-unit oscillatory activity as defined by autocorrelation and crosscorrelation analyses (Bergman et al. 1994; Hutchison 1997; Levy et al. 2000, 2001, 2002; Magarinos-Ascone et al. 2000; Raz et al. 2000; Steigerwald et al. 2008; Seifreid et al. 2012). Earlier studies have reported that multi-unit crosscorrelation might be a more sensitive detector of neuronal relationships than single-unit crosscorrelation (Bedenbaugh and Gerstein 1997; Gerstein 2000). Besides, in Parkinsonian patients, investigation of the relation between the STN single-unit oscillatory activity and the local background oscillatory activity revealed that most of the oscillatory neurons coherently oscillate with their neuronal background (Moran et al. 2008). In line with this view, we showed that the power spectral density analysis conducted on the spike train of the better-isolated units revealed neuronal oscillatory properties very similar to those obtained from multi-unit signals. Therefore, we have

considered that the surrounding multi-unit oscillatory activity is a better representative of the oscillatory properties of the local environment of the STN neurons.

Using this method, we confirmed that oscillatory neuronal activity, especially in the beta range, is limited to the dorsolateral motor part of the Parkinsonian STN (Zaidel et al. 2010). To date, there is no evidence that beta neuronal oscillations observed in the motor cortex (Sanes and Donoghue 1993; Baker et al. 1997; Halliday et al. 1998; Baker et al. 1999; Marsden et al. 2001; Schnitzler and Gross 2005) generate beta oscillatory activity in the dorsolateral motor part of the parkinsonian STN. Therefore, in Parkinsonian patients, the limitation of beta oscillatory activity to the dorsolateral motor part of the STN appears to be a neuronal signature of PD, rather than a straightforward consequence of the massive specific motor cortical innervation of the motor area of the STN (Nambu et al. 1996; Nambu et al. 1997; Benarroch et al. 2008; Mathai and Smith 2011).

Earlier studies showed that oscillatory neurons are more frequent in the dorsolateral part than in the remaining part of the Parkinsonian STN (Weinberger et al. 2006; Seifreid et al. 2012; Lourens et al. 2013). This is in line with the particular topography of the oscillatory phenomena within the STN of Parkinsonian patients reported in our study. Besides, Seifreid et al. (2012) found a specific higher discharge rate of the oscillatory neurons compared to the non-oscillatory neurons in the dorsal third of STN of Parkinsonian patients indicating that differences in the neuronal discharge rate between STN sub-regions are pattern activity-dependent. In keeping with this view, our results provide conclusive evidence that the higher neuronal discharge rate in the DLOR compared to the VMNR is surrounding 13-30Hz beta oscillatory activity-specific. Remarkably, the neuronal discharge rate was positively correlated to the 13-30Hz beta

oscillation strength which was on average stronger in the DLOR than in the VMNR, in line with a preferential localization of the beta oscillatory single-unit activity for the dorsolateral sensorimotor part of the STN in the Parkinsonian state (Weinberger et al. 2006; Steigerwald et al. 2008). Therefore, this region-specific exaggerated beta multi-unit oscillatory activity within the STN likely explains the higher neuronal discharge rate in the DLOR of the STN of Parkinsonian patients.

The neuronal discharge rate could be used in multi-modal analysis to delineate STN sub-regions in Parkinson's disease

In Parkinsonian patients undergoing STN-DBS, identification of the STN sub-regions is essential to accurately position the DBS electrodes in the dorsolateral motor area and thus assure an optimal motor benefit while minimizing the emotional and cognitive side effects of the DBS procedure (Hergoz et al. 2004; Godinho et al. 2006; Zaidel et al. 2010). It is already well-established that abnormal oscillatory activity divides the Parkinsonian STN into two distinct electrophysiological areas, the DLOR and the VMNR (Kuhn et al. 2005; Moran et al. 2008; Zaidel et al. 2009, 2010; Seifreid et al. 2012; Lourens et al. 2013). Therefore, automatic methods based on the RMS and PSD of the STN multi-unit signal recorded in Parkinsonian patients have already been used to delimit the outer boundaries of the STN as well as the intra-STN (dorsolateral-ventromedial) boundary during STN-DBS surgery (Moran et al. 2006; Zaidel et al. 2009). In this study, we provide conclusive evidence for a higher neuronal discharge rate in the motor area compared to the associative/limbic area of STN of Parkinsonian patients. Our results suggest that the neuronal discharge rate of the STN neurons could be

implemented, with measures of discharge pattern and synchronization, as an additional electrophysiological parameter in these automatic methods. We are fully aware that the small significant difference in the neuronal discharge rate of ~5 spikes/s between the DLOR and VMNR cannot be used online as a single feature to delineate the STN sub-regions. However, we believe that multi-modal analysis of the STN trajectory (including discharge rate, pattern and synchronization of activity as well as evoked behavioral responses and effects of electrical stimulation) could be used in the near future in order to refine the delineation of the functional STN sub-regions and the positioning of the DBS electrodes in the motor area of the STN of Parkinsonian patients.

Acknowledgements

We thank our patients for their agreement to participate in the study and to use their electrophysiological recordings.

Grants

This work was supported by the Fyssen Foundation and the Edmond and the Lily Safra Center (ELSC) to M.D., the Marie Curie Actions Fellowship (FP7 framework) to P.H., the Simone and Bernard Guttman chair of Brain Research and the generous support of the Rosetrees and Dekker Foundations to H.B and the Parkinson's At The Hadassah (PATH) and Bloom Foundations of London to Z.I.

Disclosure

There is no conflict of interest from any of the authors.

References

Albin RL, Young AB, Penney JB. The functional anatomy of basal ganglia disorders. *Trends Neurosci* 12: 366-375, 1989.

Alexander GE, DeLong MR, Strick PL. Parallel organization of functionally segregated circuits linking basal ganglia and cortex. *Annu Rev Neurosci* 9: 357-381,1986.

Amit DJ, Brunel N. Model of global spontaneous activity and local structured activity during delay periods in the cerebral cortex. *Cereb Cortex* 7: 237-252, 1997.

Baker SN, Olivier E, Lemon RN. Coherent oscillations in monkey motor cortex and hand muscle EMG show task-dependent modulation. *J Physiol* 501 (Pt 1): 225-241, 1997.

Baker SN, Kilner JM, Pinches EM, Lemon RN. The role of synchrony and oscillations in the motor output. *Exp Brain Res* 128: 109-117, 1999.

Bedenbaugh P, Gerstein GL. Multiunit normalized cross correlation differs from the average single-unit normalized correlation. *Neural Comput* 9: 1265-1275, 1997.

Benarroch EE. Subthalamic nucleus and its connections: Anatomic substrate for the network effects of deep brain stimulation. *Neurology* 70: 1991-1995, 2008.

Bergman H, Wichmann T, DeLong MR. Reversal of experimental parkinsonism by lesions of the subthalamic nucleus. *Science* 249:1436-1438, 1990.

Bergman H, Wichmann T, Karmon B, DeLong MR. The primate subthalamic nucleus. II. Neuronal activity in the MPTP model of parkinsonism. *J Neurophysiol* 72: 507-520, 1994.

Brown P. Oscillatory nature of human basal ganglia activity: relationship to the pathophysiology of Parkinson's disease. *Mov Disord* 18: 357-363, 2003.

Bruck A, Aalto S, Nurmi E, Vahlberg T, Bergman J, Rinne JO. Striatal subregional 6-[18F]fluoro-L-dopa uptake in early Parkinson's disease: a two-year follow-up study. *Mov Disord* 21: 958-963, 2006.

DeLong MR. Primate models of movement disorders of basal ganglia origin. *Trends Neurosci* 13: 281-285, 1990.

Difiglia M, Pasik P, Pasik T. A Golgi and ultrastructural study of the monkey globus pallidus. *J Comp Neurol* 212: 53-75, 1982.

Dunn JC. A fuzzy relative of the ISODATA process and its use in detecting compact well-separated clusters. *Journal of Cybernetics* 3(3): 32-57, 1973.

Eitan R, Shamir RR, Linetsky E, Rosenbluh O, Moshel S, Ben-Hur T, Bergman H, Israel Z. Asymetric right/left encoding of emotions in the human subthalamic nucleus. *Front Syst Neurosc* 7: 69. doi:10.3389 / fnsys. 2013.00069, 2013.

Francois C, Yelnik J, Percheron G. Golgi study of the primate substantia nigra. II. Spatial organization of dendritic arborizations in relation to the cytoarchitectonic boundaries and to the striatonigral bundle. *J Comp Neurol* 265: 473-493, 1987.

Gerstein GL. Cross-correlation measures of unresolved multi-neuron recordings. *J Neurosci Methods* 100: 41-51, 2000.

Godinho F, Thobois S, Magnin M, Guenot M, Polo G, Benatru I, Xie J, Salvetti A, Garcia-Larrea L, Broussolle E, Mertens P. Subthalamic nucleus stimulation in Parkinson's disease : anatomical and electrophysiological localization of active contacts. *J Neurol* 253: 1347-1355, 2006.

Haber SN, Lynd-Balta E, Mitchell SJ. The organization of the descending ventral pallidal projections in the monkey. *J Comp Neurol* 329: 111-128, 1993.

Halliday DM, Conway BA, Farmer SF, Rosenberg JR. Using electroencephalography to study functional coupling between cortical activity and electromyograms during voluntary contractions in humans. *Neurosci Lett* 241: 5-8, 1998.

Haynes WI, Haber SN. The organization of prefrontal-subthalamic inputs in primates provides an anatomical substrate for both functional specificity and integration: implications for Basal Ganglia models and deep brain stimulation. *J Neurosci* 33: 4804-4814, 2013.

Herzog J, Fietzek U, Hamel W, Morsnowski A, Steigerwald F, Schrader B, Weinert D, Pfister G, Muller D, Mehdorn HM, Deuschl G, Volkmann J. Most effective stimulation site in subthalamic deep brain stimulation for Parkinson's disease. *Mov Disord* 19: 1050-1054, 2004.

Hill DN, Mehta SB, Kleinfeld D. Quality metrics to accompany spike sorting of extracellular signals. *J Neurosci* 31: 8699-8705, 2011.

Hutchison WD, Lozano AM, Tasker RR, Lang AE, Dostrovsky JO. Identification and characterization of neurons with tremor-frequency activity in human globus pallidus. *Exp Brain Res* 113: 557-563, 1997.

Hutchison WD, Allan RJ, Opitz H, Levy R, Dostrovsky JO, Lang AE, Lozano AM. Neurophysiological identification of the subthalamic nucleus in surgery for Parkinson's disease. *Ann Neurol* 44: 622-628, 1998.

Joshua M, Elias S, Levine O, Bergman H. Quantifying the isolation quality of extracellularly recorded action potentials. *J Neurosci Methods* 163: 267-282, 2007.

Karachi C, Yelnik J, Tande D, Tremblay L, Hirsch EC, Francois C. The pallidosubthalamic projection: an anatomical substrate for nonmotor functions of the subthalamic nucleus in primates. *Mov Disord* 20: 172-180, 2005.

Kish SJ, Shannak K, Hornykiewicz O. Uneven pattern of dopamine loss in the striatum of patients with idiopathic Parkinson's disease. Pathophysiologic and clinical implications. *N Engl J Med* 318: 876-880, 1988.

Kuhn AA, Trottenberg T, Kivi A, Kupsch A, Schneider GH, Brown P. The relationship between local field potential and neuronal discharge in the subthalamic nucleus of patients with Parkinson's disease. *Exp Neurol* 194: 212-220, 2005.

Levy R, Hutchison WD, Lozano AM, Dostrovsky JO. High-frequency synchronization of neuronal activity in the subthalamic nucleus of parkinsonian patients with limb tremor. *J Neurosci* 20: 7766-7775, 2000.

Levy R, Dostrovsky JO, Lang AE, Sime E, Hutchison WD, Lozano AM. Effects of apomorphine on subthalamic nucleus and globus pallidus internus neurons in patients with Parkinson's disease. *J Neurophysiol* 86: 249-260, 2001.

Levy R, Hutchison WD, Lozano AM, Dostrovsky JO. Synchronized neuronal discharge in the basal ganglia of parkinsonian patients is limited to oscillatory activity. *J Neurosci* 22: 2855-2861, 2002.

Lewicki MS. A review of methods for spike sorting: the detection and classification of neural action potentials. *Network* 9: R53-R78, 1998.

Lourens MA, Meijer HG, Contarino MF, van den Munckhof P, Schuurman PR, van Gils SA, Bour LJ. Functional neuronal activity and connectivity within the subthalamic nucleus in Parkinson's disease. *Clin Neurophysiol* 124: 967-981, 2013.

Machado A, Rezai AR, Kopell BH, Gross RE, Sharan AD, Benabid AL. Deep brain stimulation for Parkinson's disease: surgical technique and perioperative management. *Mov Disord* 21 Suppl 14: S247-S258, 2006.

Magarinos-Ascone CM, Figueiras-Mendez R, Riva-Meana C, Cordoba-Fernandez A. Subthalamic neuron activity related to tremor and movement in Parkinson's disease. *Eur J Neurosci* 12: 2597-2607, 2000.

Mallet N, Pogosyan A, Sharott A, Csicsvari J, Bolam JP, Brown P, Magill PJ. Disrupted dopamine transmission and the emergence of exaggerated beta oscillations in subthalamic nucleus and cerebral cortex. *J Neurosci* 28: 4795-4806, 2008.

Marsden JF, Limousin-Dowsey P, Ashby P, Pollak P, Brown P. Subthalamic nucleus, sensorimotor cortex and muscle interrelationships in Parkinson's disease. *Brain* 124: 378-388, 2001.

Mathai A, Smith Y. The corticostriatal and corticosubthalamic pathways: two entries, one target. So what? *Front Syst Neurosci* 5: 64, 2011.

Moran A, Bar-Gad I, Bergman H, Israel Z. Real-time refinement of subthalamic nucleus targeting using Bayesian decision-making on the root mean square measure. *Mov Disord* 21: 1425-1431, 2006.

Moran A, Bergman H, Israel Z, Bar-Gad I. Subthalamic nucleus functional organization revealed by parkinsonian neuronal oscillations and synchrony. *Brain* 131: 3395-3409, 2008.

Moran A, Bar-Gad I. Revealing neuronal functional organization through the relation between multi-scale oscillatory extracellular signals. *J Neurosci Methods* 186: 116-129, 2010.

Morrish PK, Sawle GV, Brooks DJ. Regional changes in [18F]dopa metabolism in the striatum in Parkinson's disease. *Brain* 119 (Pt 6): 2097-2103, 1996.

Moshel S, Shamir RR, Raz A, Ramirez de Noriega F, Eitan R, Bergman H, Israel Z. Subthalamic nucleus long-range synchronization - an independent hallmark of human Parkinson's disease. *Front Syst Neurosc* 7: 79. doi:10.3389 / fnsys. 2013.00079, 2013.

Nambu A, Takada M, Inase M, Tokuno H. Dual somatotopical representations in the primate subthalamic nucleus: evidence for ordered but reversed body-map transformations from the primary motor cortex and the supplementary motor area. *J Neurosci* 16: 2671-2683, 1996.

Nambu A, Tokuno H, Inase M, Takada M. Corticosubthalamic input zones from forelimb representations of the dorsal and ventral divisions of the premotor cortex in the macaque monkey: comparison with the input zones from the primary motor cortex and the supplementary motor area. *Neurosci Lett* 239: 13-16, 1997.

Nurmi E, Ruottinen HM, Bergman J, Haaparanta M, Solin O, Sonninen P, Rinne JO. Rate of progression in Parkinson's disease: a 6-[18F]fluoro-L-dopa PET study. *Mov Disord* 16: 608-615, 2001.

Parent A, Hazrati LN. Functional anatomy of the basal ganglia. I. The cortico-basal ganglia-thalamo-cortical loop. *Brain Res Brain Res Rev* 20: 91-127, 1995.

Raz A, Vaadia E, Bergman H. Firing patterns and correlations of spontaneous discharge of pallidal neurons in the normal and the tremulous 1-methyl-4-phenyl-1,2,3,6-tetrahydropyridine vervet model of parkinsonism. *J Neurosci* 20: 8559-8571, 2000.

Remple MS, Bradenham CH, Kao CC, Charles PD, Neimat JS, Konrad PE. Subthalamic nucleus neuronal firing rate increases with Parkinson's disease progression. *Mov Disord* 26: 1657-1662, 2011.

Rodriguez-Oroz MC, Rodriguez M, Guridi J, Mewes K, Chockkman V, Vitek J, DeLong MR, Obeso JA. The subthalamic nucleus in Parkinson's disease: somatotopic organization and physiological characteristics. *Brain* 124: 1777-1790, 2001.

Rousseeuw PJ. Silhouettes: a graphical aid to the interpretation and validation of cluster analysis. *J Comput Appl Math* 20: 53-65, 1987.

Sanes JN, Donoghue JP. Oscillations in local field potentials of the primate motor cortex during voluntary movement. *Proc Natl Acad Sci U S A* 90: 4470-4474, 1993.

Schnitzler A, Gross J. Normal and pathological oscillatory communication in the brain. *Nat Rev Neurosci* 6: 285-296, 2005.

Seifried C, Weise L, Hartmann R, Gasser T, Baudrexel S, Szelenyi A, van de Loo S, Steinmetz H, Seifert V, Roeper J, Hilker R. Intraoperative microelectrode recording for the delineation of subthalamic nucleus topography in Parkinson's disease. *Brain Stimul* 5: 378-387, 2012.

Shadlen MN, Newsome WT. Noise, neural codes and cortical organization. *Curr Opin Neurobiol* 4: 569-579, 1994.

Sharott A, Magill PJ, Harnack D, Kupsch A, Meissner W, Brown P. Dopamine depletion increases the power and coherence of beta-oscillations in the cerebral cortex and subthalamic nucleus of the awake rat. *Eur J Neurosci* 21: 1413-1422, 2005.

Shink E, Smith Y. Differential synaptic innervation of neurons in the internal and external segments of the globus pallidus by the. *J Comp Neurol* 358: 119-141, 1995.

Steigerwald F, Potter M, Herzog J, Pinsker M, Kopper F, Mehdorn H, Deuschl G, Volkmann J. Neuronal activity of the human subthalamic nucleus in the parkinsonian and nonparkinsonian state. *J Neurophysiol* 100: 2515-2524, 2008.

Stein E, Bar-Gad I. beta oscillations in the cortico-basal ganglia loop during parkinsonism. *Exp Neurol* 245: 52-59, 2013.

Tan AY, Chen Y, Scholl B, Seidemann E, Priebe NJ. Sensory stimulation shifts visual cortex from synchronous to asynchronous states. *Nature* 2014.

van Vreeswijk C, Sompolinsky H. Chaos in neuronal networks with balanced excitatory and inhibitory activity. *Science* 274: 1724-**1726**, 1996.

Weinberger M, Mahant N, Hutchison WD, Lozano AM, Moro E, Hodaie M, Lang AE, Dostrovsky JO. Beta oscillatory activity in the subthalamic nucleus and its relation to dopaminergic response in Parkinson's disease. *J Neurophysiol* 96: 3248-3256, 2006.

Wichmann T, Bergman H, DeLong MR. The primate subthalamic nucleus. III. Changes in motor behavior and neuronal activity in the internal pallidum induced by subthalamic inactivation in the MPTP model of parkinsonism. *J Neurophysiol* 72: 521-530, 1994.

Wichmann T, DeLong MR. Pathophysiology of Parkinson's disease: the MPTP primate model of the human disorder. *Ann N Y Acad Sci* 991: 199-213, 2003.

Wichmann T, Soares J. Neuronal firing before and after burst discharges in the monkey basal ganglia is predictably patterned in the normal state and altered in parkinsonism. *J Neurophysiol* 95: 2120-2133, 2006.

Yin HH, Knowlton BJ. The role of the basal ganglia in habit formation. *Nat Rev Neurosci* 7: 464-476, 2006.

Zaidel A, Spivak A, Shpigelman L, Bergman H, Israel Z. Delimiting subterritories of the human subthalamic nucleus by means of microelectrode recordings and a Hidden Markov Model. *Mov Disord* 24: 1785-1793, 2009.

Zaidel A, Spivak A, Grieb B, Bergman H, Israel Z. Subthalamic span of beta oscillations predicts deep brain stimulation efficacy for patients with Parkinson's disease. *Brain* 133: 2007-2021, 2010.

Tables et Figures

Table 1: Patients information

Patient No.	Sex	Age (years)	Disease duration (years)	Surgery side	Pre-operative		
					UPDRS 3 (OFF)	UPDRS 3 (ON)	LED
1	f	62	12	bilateral	32	6	925
2	m	70	10	bilateral	N/A	N/A	950
3	f	61	10	bilateral	N/A	N/A	1000
4	m	66	10	bilateral	68	27	1250
5	m	74	20	bilateral	60	16	1496
6	m	61	8	bilateral	46	21	500
7	f	65	7	bilateral	21	4	917.5
8	m	54	5	bilateral	86	42	500
9	m	62	5	bilateral	44	12	975
10	f	56	13	bilateral	N/A	N/A	N/A
11	m	49	8	bilateral	N/A	N/A	N/A
12	m	62	17	bilateral	72	22	1550
13	f	70	13	bilateral	41	13	400
14	f	70	9	unilateral, right	33	6	1875
15	m	53	9	bilateral	41	10	375
16	m	73	8	unilateral, right	N/A	N/A	1125
17	f	50	9	bilateral	N/A	N/A	550
18	f	45	9	bilateral	82	55	700
19	m	62	5	bilateral	N/A	N/A	N/A
20	m	57	11	bilateral	47	11	1120
21	m	63	14	bilateral	55	19	1005
22	m	62	7	bilateral	63	17	1080
23	m	52	5	bilateral	27	3	510
24	f	53	10	bilateral	42	9	770
25	f	74	9	unilateral, right	73	42	1250
26	m	57	7	bilateral	78	37	1370
27	m	69	10	unilateral, right	50	10	1140
28	m	67	8	unilateral, left	34	14	1000
29	m	59	10	bilateral	47	13	N/A
30	f	55	9	bilateral	57	17	580
31	m	55	8	bilateral	69	22	1480
32	m	53	8	bilateral	49	32	750
33	m	51	10	bilateral	43	29	562.5
34	m	65	6	bilateral	64	29	750
35	m	64	9	bilateral	69	48	N/A
36	f	54	6	bilateral	48	19	680
37	m	62	5	bilateral	N/A	N/A	N/A
38	m	54	3	bilateral	49	6	200
39	m	65	4	bilateral	56	34	850
40	m	74	15	bilateral	57	31	750
41	m	71	22	bilateral	51	35	2000
42	m	51	10	unilateral, right	47	35	93.7
43	m	63	30	bilateral	56	22	1120
44	f	66	3.5	bilateral	46	16	750
45	m	66	10	bilateral	63	11	600
46	m	66	N/A	unilateral, left	N/A	N/A	N/A
47	m	61	8	bilateral	32	7	750
48	f	49	14	bilateral	N/A	N/A	N/A
49	f	60	14	bilateral	75	19	1000
50	m	70	8	unilateral, right	55	13	1500
51	m	55	10	bilateral	75	41	500
52	m	64	20	bilateral	35	2	875
53	m	50	20	bilateral	53	39	N/A
54	m	64	7	bilateral	59	18	810
55	m	65	8	bilateral	48	12	750
56	m	66	N/A	unilateral, left	55	24	550
57	m	60	8	unilateral, left	48	13	570
58	f	68	15	bilateral	35	11	1147.5
59	m	65	8	unilateral, right	41	6	825
60	m	61	7	unilateral, right	85	30	870
sum / mean ± SD	44 m 16 f	61.2 ± 7.2	10.1 ± 4.9	48 bilateral 12 unilateral	53.2 ± 15.4	20.6 ± 12.9	895 ± 391.5

N/A : Not Available
UPDRS 3 (OFF/ON medication) : clinician-scored motor evaluation (range 0–108)
LED : Levopoda Equivalent Dose

Table 2: Microelectrode trajectory characteristics

Patient No.	Side	Left				Right			
		MER1		MER2		MER1		MER2	
		STN length (mm)	DLOR length/STN length (%)	STN length (mm)	DLOR length/STN length (%)	STN length (mm)	DLOR length/STN length (%)	STN length (mm)	DLOR length/STN length (%)
1	L/R	1.682	DLOR N/D	**6.714**	**60.49**	1.395	DLOR N/D	Exit N/D	"-"
2	L/R	STN N/D	"-"	5.222	DLOR N/D	**4.453**	**21.69**	**5.024**	**21.60**
3	L/R	**5.647**	**17.48**	**4.669**	**44.96**	STN N/D	"-"	**4.859**	**34.78**
4	L/R	2.095	DLOR N/D	**5.946**	**18.43**	"-"	"-"	Exit N/D	"-"
5	L/R	**5.908**	**59.65**	**5.873**	**27.21**	**4.844**	**45.31**	**6.158**	**28.91**
6	L/R	**5.725**	**52.84**	**6.735**	**49.55**	STN N/D	"-"	**5.686**	**21.07**
7	L/R	**5.654**	**41.72**	**6.266**	**26.81**	STN N/D	"-"	3.892	DLOR N/D
8	L/R	"-"	"-"	**6.199**	**80.80**	**4.923**	**89.86**	3.111	DLOR N/D
9	L/R	"-"	"-"	Exit N/D	"-"	**5.617**	**20.24**	**7.455**	**55.87**
10	L/R	STN N/D	"-"	Exit N/D	"-"	**4.257**	**39.02**	**5.407**	**36.62**
11	L/R	**4.752**	**56.38**	Exit N/D	"-"	STN N/D	"-"	**4.91**	**20.67**
12	L/R	**5.056**	**55.02**	Exit N/D	"-"	2.268	DLOR N/D	**5.954**	**29.51**
13	L/R	Exit N/D	"-"	**6.484**	**70.85**	**5.694**	**68.41**	Exit N/D	"-"
14	R	"-"	"-"	"-"	"-"	STN N/D	"-"	3.248	DLOR N/D
15	L/R	**7.538**	**67.10**	3.784	100	**4.517**	**69.89**	**5.739**	**62.21**
16	R	"-"	"-"	"-"	"-"	STN N/D	"-"	STN N/D	"-"
17	L/R	**3.99**	**29.20**	Exit N/D	"-"	**4.959**	**62.92**	**5.383**	**62.03**
18	L/R	5.597	DLOR N/D	3.92	DLOR N/D	5.497	DLOR N/D	**5.732**	**14.32**
19	L/R	STN N/D	"-"	STN N/D	"-"	STN N/D	"-"	4.921	DLOR N/D
20	L/R	**2.753**	**35.71**	Exit N/D	"-"	4.903	DLOR N/D	5.058	DLOR N/D
21	L/R	STN N/D	"-"	6.972	DLOR N/D	**4.224**	**8.95**	**5.936**	**39.59**
22	L/R	3.518	DLOR N/D	**7.159**	**44.07**	4.782	DLOR N/D	Exit N/D	"-"
23	L/R	"-"	"-"	**3.207**	**65.67**	2.303	DLOR N/D	Exit N/D	"-"
24	L/R	"-"	"-"	**3.573**	**80.35**	**4.822**	**81.13**	Exit N/D	"-"
25	R	"-"	"-"	"-"	"-"	**5.006**	**37.97**	1.503	DLOR N/D
26	L/R	**5.97**	**36.53**	**4.375**	**50.31**	**6.786**	**48.57**	**5.689**	**66.76**
27	R	"-"	"-"	"-"	"-"	**2.694**	**7.42**	**5.951**	**78.26**
28	L	Exit N/D	"-"	Exit N/D	"-"	"-"	"-"	"-"	"-"
29	L/R	**8.184**	**53.69**	Exit N/D	"-"	**6.613**	**42.25**	Exit N/D	"-"
30	L/R	Exit N/D	"-"	**2.154**	**37.09**	**5.998**	**18.36**	STN N/D	"-"
31	L/R	**5.076**	**3.94**	**2.618**	**84.72**	Exit N/D	"-"	**5.583**	**55.13**
32	L/R	**3.38**	**11.63**	STN N/D	"-"	**5.373**	**25.85**	2.987	DLOR N/D
33	L/R	Exit N/D	"-"	**5.991**	**62.29**	**6.586**	**55.97**	**6.385**	**39.12**
34	L/R	**4.743**	**63.21**	STN N/D	"-"	**6.499**	**76.84**	**5.143**	**84.43**
35	L/R	**6.122**	**67.45**	**3.517**	**66.02**	**4.414**	**77.96**	Exit N/D	"-"
36	L/R	**4.984**	**70.02**	STN N/D	"-"	**6.579**	**64.92**	Exit N/D	"-"
37	L/R	**6.05**	**25.72**	**7.38**	**17.47**	**5.912**	**28.57**	Exit N/D	"-"
38	L/R	Exit N/D	"-"	**3.495**	**57.25**	**5.696**	**70.10**	**5.492**	**69.01**
39	L/R	**3.662**	**70.32**	**5.202**	**22.93**	**4.585**	**12.93**	**5.562**	**4.93**
40	L/R	Exit N/D	"-"	Exit N/D	"-"	**5.368**	**55.46**	**5.513**	**78.56**
41	L/R	STN N/D	"-"	**5.803**	**43.99**	Exit N/D	"-"	Exit N/D	"-"
42	R	"-"	"-"	"-"	"-"	**5.209**	**61.68**	**4.015**	**82.52**
43	L/R	STN N/D	"-"	**5.972**	**46.48**	4.097	DLOR N/D	**5.997**	**31.67**
44	L/R	4.535	DLOR N/D	7.529	DLOR N/D	**4.737**	**35.30**	4.843	DLOR N/D
45	L/R	**4.966**	**45.93**	**6.752**	**60.07**	**5.226**	**57.46**	**3.641**	**24.61**
46	L	STN N/D	"-"	**6.337**	**66.96**	"-"	"-"	"-"	"-"
47	L/R	STN N/D	"-"	STN N/D	"-"	4.496	DLOR N/D	5.895	DLOR N/D
48	L/R	**5.876**	**42.09**	**5.455**	**34.35**	**5.993**	**49.99**	**4.694**	**51.07**
49	L/R	**2.004**	**74.87**	**5.656**	**73.59**	**5.999**	**78.28**	4.49	100
50	R	"-"	"-"	"-"	"-"	**4.313**	**9.09**	3.566	DLOR N/D
51	L/R	**5.968**	**48.22**	**5.39**	**74.04**	4.371	DLOR N/D	**5.627**	**66.95**
52	L/R	**6.738**	**24.90**	**2.187**	**40.97**	"-"	"-"	Exit N/D	"-"
53	L/R	**6.544**	**16.61**	**5.448**	**7.12**	5.795	DLOR N/D	**5.697**	**64.77**
54	L/R	**6.894**	**39.37**	**5.234**	**48.40**	**5.763**	**53.15**	STN N/D	"-"
55	L/R	"-"	"-"	**6.187**	**4.78**	6.117	DLOR N/D	Exit N/D	"-"
56	L	**5.467**	**61.92**	**3.684**	**86.40**	"-"	"-"	"-"	"-"
57	L	7.049	DLOR N/D	6.442	DLOR N/D	"-"	"-"	"-"	"-"
58	L/R	**2.589**	**57.51**	**6.479**	**45.96**	Exit N/D	"-"	**4.224**	**55.16**
59	R	"-"	"-"	"-"	"-"	2.198	DLOR N/D	Exit N/D	"-"
60	R	"-"	"-"	"-"	"-"	**6.512**	**75.38**	**4.808**	**75.00**
sum / mean ± SD	48 bilateral 12 unilateral	**5.27 ± 1.47**	**45.52 ± 19.72**	**5.25 ± 1.47**	**50.01 ± 22.38**	**5.32 ± 0.92**	**48.47 ± 24.14**	**5.44 ± 0.76**	**48.40 ± 22.96**

STN N/D : STN Not Detected, Hidden Markov Model method did not detect STN entry over the microelectrode trajectory
Exit N/D : STN Exit Not Detected, Hidden Markov Model method did not detect STN exit over the microelectrode trajectory
DLOR N/D : DLOR Not Detected, Hidden Markov Model method did not detect increase of beta oscillatory activity within the STN
"_" : Data do not exist. Only unilateral or one microelectrode recording
In bold, the 119 STN microelectrode trajectories with clear STN entry and exit and discerible DLOR and VMNR, using the Hidden Markov Model method

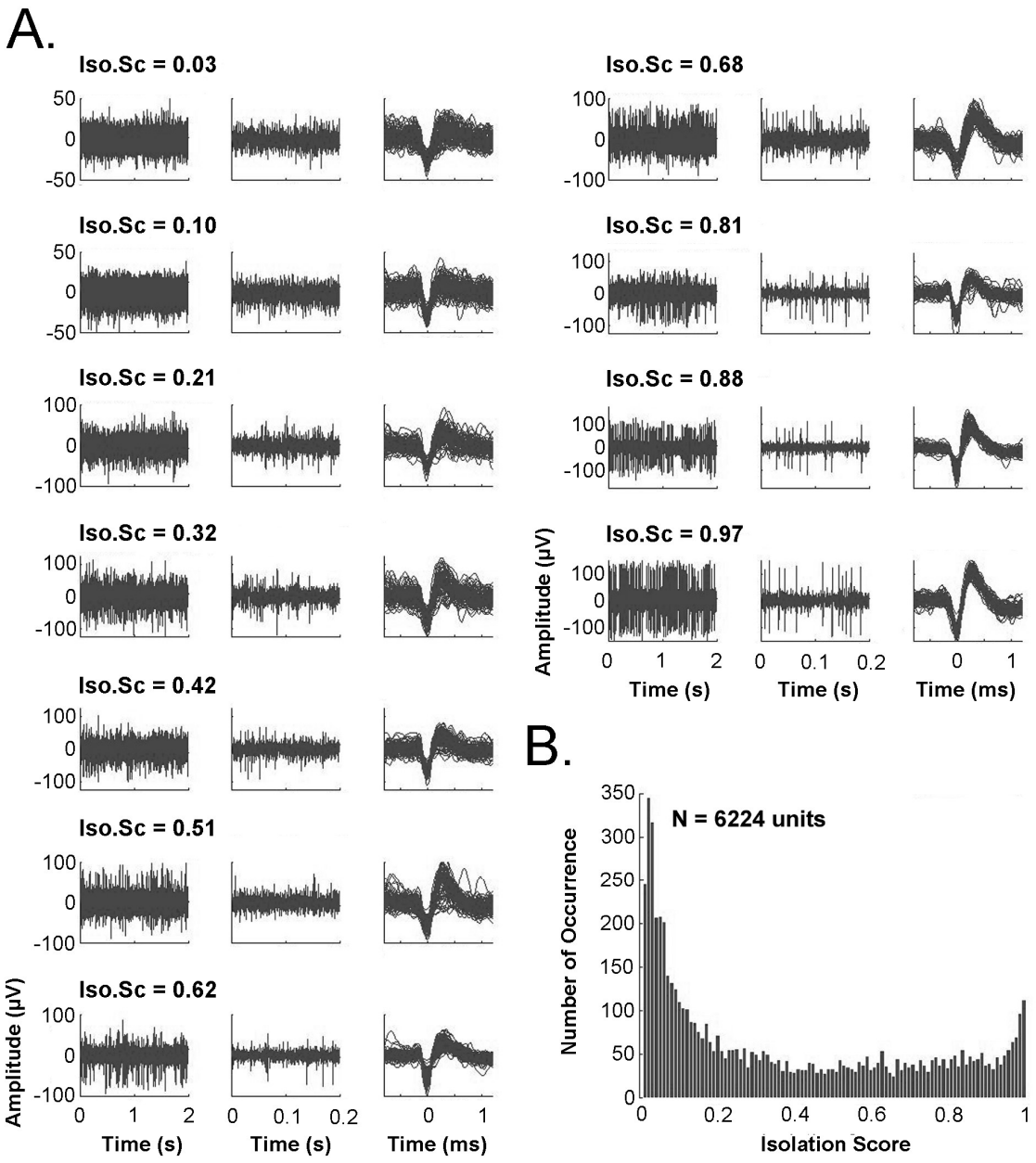

Figure 1. Spike sorting examples and single-unit database. Examples of 2s **(A.left)** and 200ms **(A.middle)** STN multi-unit recordings and 100 superimposed waveforms of the extracellular action potentials of an identified unit sorted from its multi-unit activity **(A.right)**. The waveforms were randomly selected from the whole stable recorded period.

Iso.Sc indicates the isolation score of the identified unit sorted from its multi-unit activity. **(B)** Distribution of the isolation score of all the identified units (N = 6224).

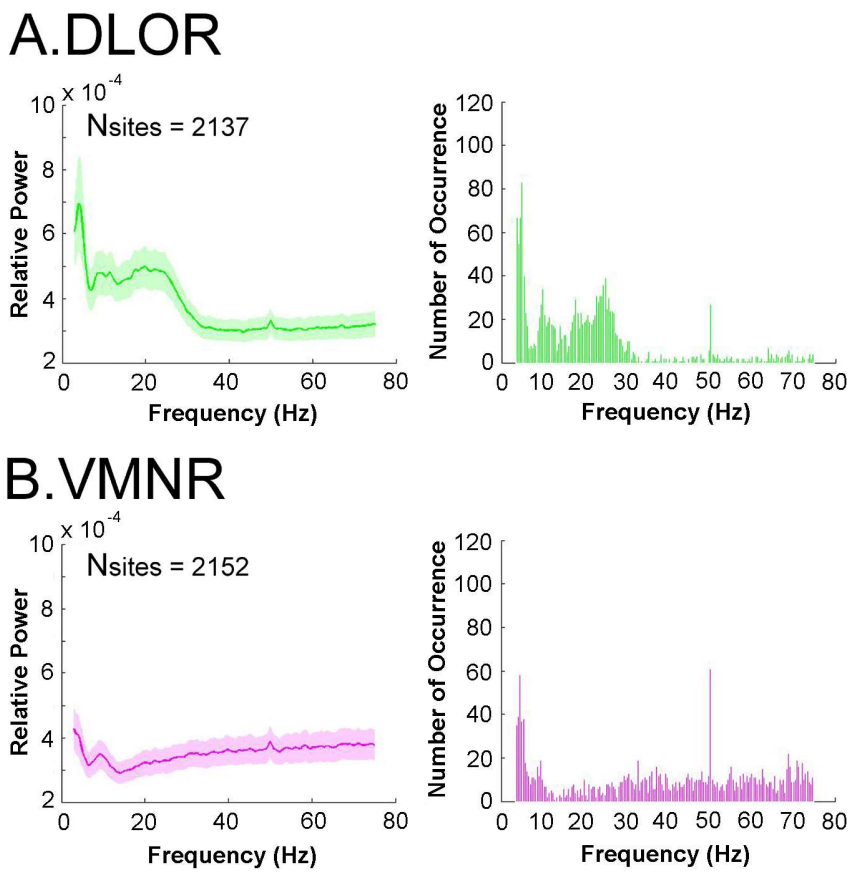

Figure 2. Predominant oscillatory activity in STN DLOR. Mean PSD of STN multi-unit activity of DLOR **(A.left)** and VMNR **(B.left)** recordings. The shaded areas mark SEMs. Nsites is the number of recording sites averaged. Distribution of f_{peak} (the frequency at which the PSD attains its maximal value) of all the PSDs of STN multi-unit activity of the DLOR **(A.right)** and VMNR **(B.right)** recordings.

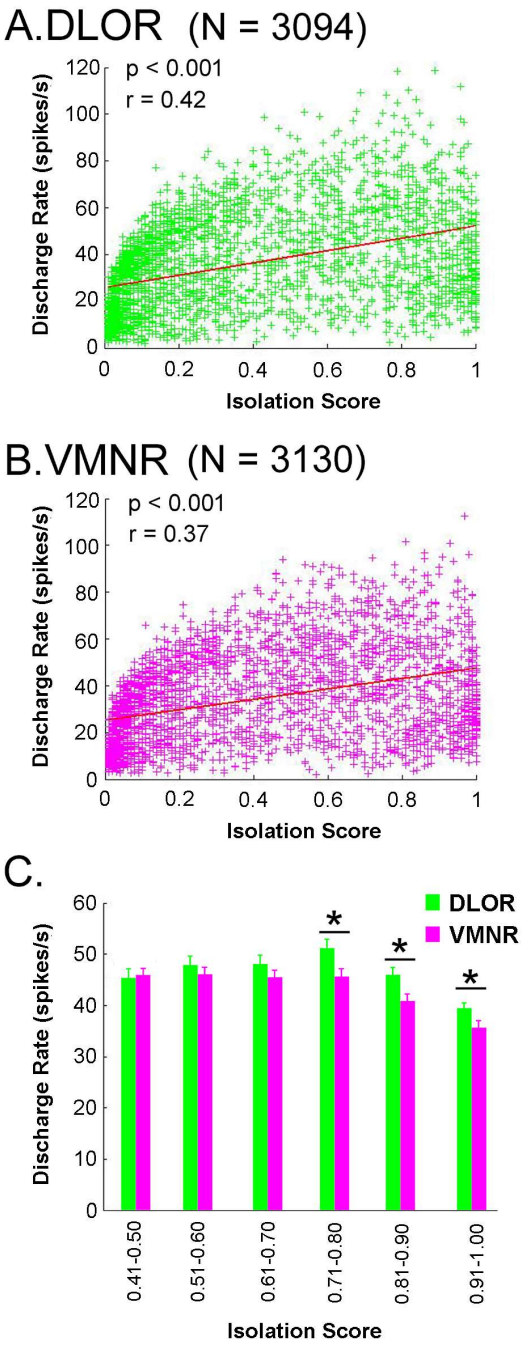

Figure 3. Higher neuronal discharge rate in STN DLOR for the better-isolated units. Scatter plots of the neuronal discharge rate and the isolation score of all the identified STN units located in the DLOR **(A)** and VMNR **(B)**. N is the number of

identified STN units. Black line represents the linear regression line between the discharge rate of the STN units and their isolation score. r is the Pearson correlation coefficient and p indicates the probability that r = 0. **(C)** Mean neuronal discharge rate in the DLOR and VMNR calculated depending on the different isolation score ranges of the STN units. Error bars represent SEMs. * indicates significant ($P < 0.05$) differences between the DLOR and VMNR discharge rates.

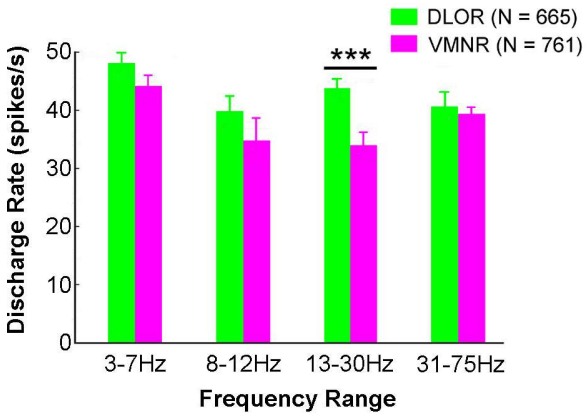

Figure 4. Higher neuronal discharge rate in STN DLOR for surrounding beta multi-unit oscillatory activity. Mean discharge rate of the better-isolated STN units (isolation score > 0.70) in the DLOR and VMNR depending on the f_{peak} ranges of their multi-unit oscillatory activity: 3-7Hz theta range, 8-12Hz alpha range, 13-30Hz beta range and >30Hz gamma band. N is the total number of better-isolated STN units averaged. Error bars represent SEMs. *** indicates significant ($P < 0.001$) differences between the DLOR and VMNR discharge rates.

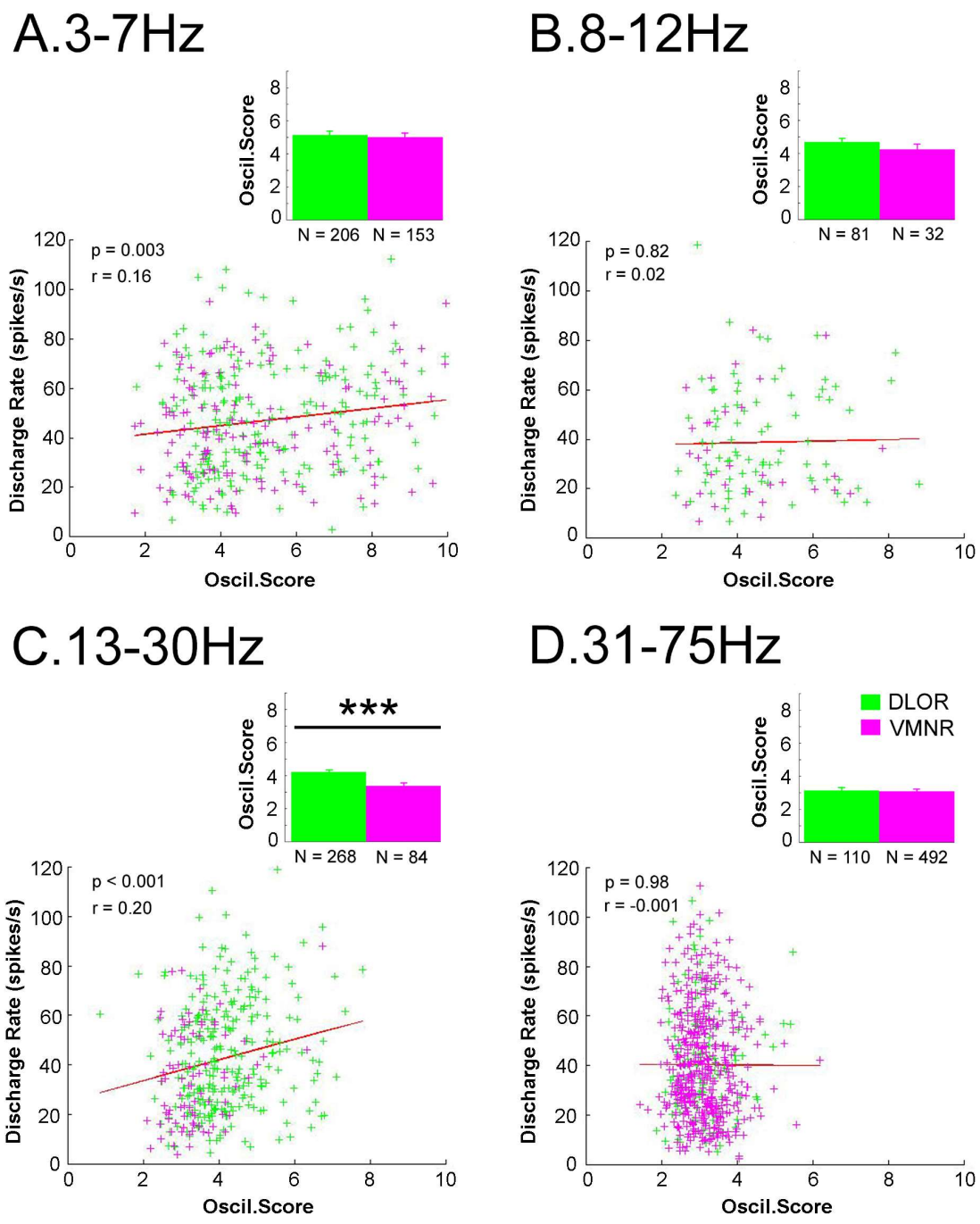

Figure 5. Positive correlation between the discharge rate of the STN neurons and the strength of their surrounding oscillatory activity, especially at the beta frequencies. Scatter plots of the discharge rate of the better-isolated STN units and the

Oscil.Score of their multi-unit oscillatory activity depending on the corresponding f_{peak} ranges: 3-7Hz theta range **(A)**, 8-12Hz alpha range **(B)**, 13-30Hz beta range **(C)** and >30Hz gamma band **(D)**. Same conventions as in Figure 3.A and 3.B. Mean *Oscil.Score* calculated depending on the different f_{peak} ranges in the DLOR and VMNR is inset in each scatter plot. Same conventions as in Figure 4.